May 26, 2020

Study of WW $\to q\bar{q}\ell\nu$ at ILC500 with ILD

JUSTIN ANGUIANO[1]

Department of Physics and Astronomy
University of Kansas, Lawrence, KS 66045, U.S.A.

The study showcases the approaches towards lepton identification and pileup mitigation at center-of-mass energy $\sqrt{s} = 500$ GeV for semileptonic WW decays at ILC. The analysis is performed using fully simulated Standard Model Monte Carlo events with the ILD detector concept and emphasizes the measurement of the W mass. The mass measurement is performed through the identification of a lepton and treatment of the remaining system as the hadronic W-boson. Only the most favorable beam polarization scenario for WW production is considered. The resulting detector performance benchmark obtained with an integrated luminosity of 1600 fb^{-1} is the statistical error of the W mass $\Delta M_W(\text{stat.}) = 2.4$ MeV and a relative statistical error on the WW cross-section $\Delta\sigma/\sigma(\text{stat.}) = 0.038\%$.

Talk presented at

The International Workshop on Future Linear Colliders
(LCWS19),
Sendai, Japan, 2-6?? November 2019

[1]Work supported by the National Science Foundation under award PHY-1306953.

1 Introduction and motivation

The W-boson pair decaying semileptonically is a rich physics channel with a wide variety of facets to study. The most well motivated is the measurement of the W mass because of the easy identification of the lepton which automatically tags the hadronic W as the remaining particles in the system. The mass measurement quality is then only bounded by the performance of the detector. WW production is also sensitive to the polarization of electron positron collider beams. Measuring the production cross section implicity measures the beam polarization at the interaction point. Another important aspect of WW, is the charged triple gauge couplings(TGCs). Deviation of these couplings with the Standard Model is a distinct signature of new physics. This study assesses the challenges associated with reconstruction and analysis of semileptonic W pairs at center of mass energy 500 GeV, which is an important tool in understanding the problems that lie in analysis within the next frontier of particle physics. The work presented contains four major steps. The first step is the identification of the lepton, which is done with a universal treatment of leptons, that is, without distinguishing between types of leptons. Second, the effects of pileup on the hadronic mass are explored and a technique to reduce this effect is showcased. Third is the event selection where W pairs are selected against the full standard model background. Lastly, measurements for the statistical error of the W mass and cross section are extracted.

2 Physics

2.1 The Standard Model

— *The W-boson*
The most difficult reconstruction of a final state from W decay is the case of a tau lepton. The tau can mimic the signature of hadrons or other leptons in a detector in addition to producing additional missing energy via neutrinos. The tau has a shorter lifetime compared to the other charged leptons and flies a short distance before decaying. If produced from the interaction point in a detector, the tau will travel on average $87\,\mu$m before decaying. The other leptons, like the electron, is stable and doesn't decay, and the muon is not stable but is unlikely to decay inside the detector. The tau lepton mainly decays hadronically – into a tau neutrino and virtual W-boson that produces a pair of quarks. The virtual W's daughter quarks will hadronize into a charged particle ($\pi^{\pm}$) or radiate more quarks that form either more charged or neutral particles (π^0). If π^0's are created they immediately decay mostly into two photons. When a tau produces a single charged particle this is classified as a 1-prong decay, 3 charged particles is classified as a 3-prong decay. The virtual W in the tau decay is allowed to couple with leptons, so, the tau final state can include

either an electron or muon along with the corresponding flavor neutrinos. The decay rates for the tau are given in Table 1.

	Decay Mode	Branching Ratio
Hadronic Modes (64.79%)	$\pi^-\nu_\tau$	10.82%
	$\pi^-\pi^0\nu_\tau$	25.49%
	$\pi^-\pi^0\pi^0\nu_\tau$	9.26%
	$\pi^-\pi^0\pi^0\pi^0\nu_\tau$	1.04%
	$\pi^-\pi^+\pi^-\nu_\tau$	8.99%
	$\pi^-\pi^+\pi^-\pi^0\nu_\tau$	2.74%
Leptonic Modes (35.21%)	$e^-\nu_e\nu_\tau$	17.82%
	$\mu^-\nu_\mu\nu_\tau$	17.39%

Table 1: Most common decay modes for the τ^- lepton [1]

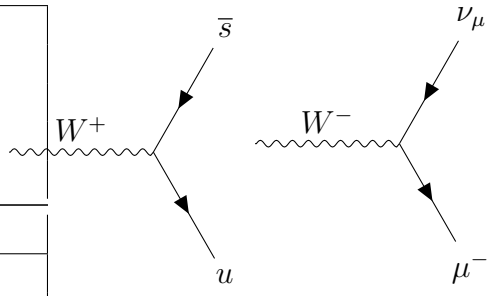

Figure 1: Fundamental vertices between the W-boson and fermions

— *The W Mass*

The W-boson is an unstable particle and abides by a total decay rate $\Gamma = 1/\tau$ where τ is the average lifetime. A consequence of this decay length is that the observed mass distribution will approximately follow a Breit-Wigner distribution. The mass distribution is centered on the nominal W mass M_W with a width characterized by the full width half maximum Γ_W. The current highest precision measurement for the mass and width are results of measurements through single $W^\pm$ production. These measurements use the combined results from LEP and Tevatron experiments which reports $M_W = 80.379 \pm 0.012$ GeV and $\Gamma_W = 2.085 \pm 0.042$ GeV [1]. The diagrams representing WW are given in Figure 2. The final states of the WW process are either the fully hadronic $WW \to q\overline{q}q\overline{q}$, semileptonic $WW \to q\overline{q}\ell\nu_\ell$, or fully leptonic $WW \to \ell\nu\ell\nu$. The semileptonic mode is the most favorable way to measure the W mass because the hadronic system is easily obtained after the identification of the lepton. The hadronic mode is more challenging due to the combinatoric assignment of the four hadronic jets into two W's along with color-reconnection which may cause "cross-talk" between jets. The leptonic channel is also difficult because of the presence of two neutrinos.

2.2 The Anatomy of an Event

— *Beam effects*

Figure 2 illustrates the production of WW through $e^-\,e^+$ annihilation. Within the collider annihilation presents two important effects: beamstrahlung and pile-up. The first is related to photons produced from the interactions between the fields of the

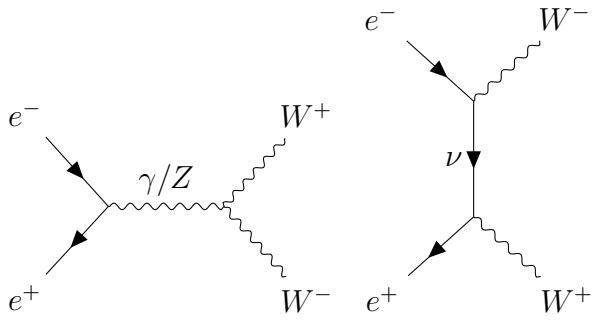

Figure 2: Main WW production modes in the s and t channels.

beams. The radiated photons generally go undetected by escaping down the beam-pipe causing the effective center of mass energy to be reduced at the interaction point. There is a significant probability that these photons will interact with other photons or beam particles and produce hadrons that scatter into the detector and mix in with the event of interest. These particles add a source of confusion wherein the foreign particles "pile-up" ontop of the true particles of an event, thus trying to resolve the true particles of the event becomes more challenging.

— *Helicity*

The second underlying physics property in every event is related to the helicity(spin) of the interacting electron and positron. There are four possible combinations of electron and positron helicities where each initial particle is either left or right handed. More explicitly, a collision can consist of $e^-_L e^+_R$(LR) with left-handed electron and right-handed positron , $e^-_R e^+_L$(RL) with right handed electron and left handed positron, or mirroring helicities RR and LL. The beams in the collider are mixed with multiple helicities which is represented by overall partial longitudinal beam polarizations P_{e^-} P_{e^+}. A diagram of possible tree-level spin configuration is shown in Figure 3. In the s-channel, the electron positron helicities are directly coupled, therefore, two W-bosons can only be produced in LR and RL configurations, whereas in the mirrored configuration the recombination into particle of spin 1 is not possible. In the t-channel diagrams, the W's are directly coupled to the beam particles. The W has pure coupling only to left handed electrons or right handed positrons so the number of WW events produced are sensitive to the beam polarization [2]. If the number of events produced is sensitive to polarization then the overall cross-section for WW production is sensitive to beam polarization.

— *Cross-section*

The cross-section is an important measurement because it verifies consistency with the underlying standard model predictions for the rate at which a process occurs. This measurement is doubly important for the WW process because it implicitly provides an in situ measurement of the beam polarizations. By definition, the cross-section

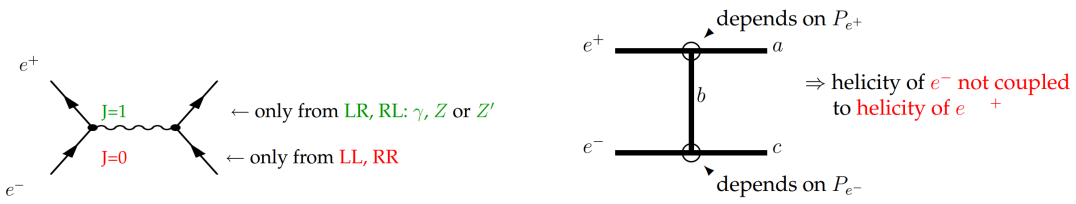

Figure 3: Possible spin configurations in the s and t channel. [3]

is a cross-sectional area and represents the probability of an interaction. The total number of events N observed for a process is given by $N = \sigma L$ with the cross-section denoted by σ and L is the integrated luminosity which is a measure of the total number of collisions. In a physics analysis the desired process(signal) is accompanied by other processes(background) that can unfortunately not be clearlly distinguished from the signal events. Topological or kinematic cuts are applied to each event to minimize the contamination of background events that enter the signal region when trying to count the number of signal events. This reduces the number of observed events N by the number of events lost to the event selection criteria. Thus the number of events observed is then

$$N = \sigma L \epsilon \tag{1}$$

where ϵ is the efficiency of the signal selection in Monte Carlo simulation. The signal efficiency is defined as:

$$\epsilon = \frac{\text{The number of signal events that pass selection}}{\text{The total number of signal events that can be selected}} \tag{2}$$

One thing to note is that for a specific process the cross-section includes contributions from all Feynman diagrams that have the same initial and final state particles. This includes diagrams that are essentially not "signal-like". For WW, examples of these contributing diagrams are given in Figure 4.

3 The ILC and ILD

3.1 Accelerator Description

The search for new physics drives collider energies higher and higher. The current most powerful operating collider is the Large Hadron Collider(LHC) at CERN with a center of mass energy of 13 TeV. The LHC has a very busy environment with significantly more pile up from many proton-proton collisions than in an electron-positron collider. The proton is also a composite particle, and when the components of the proton collide, the type and the energy of the interaction between them is

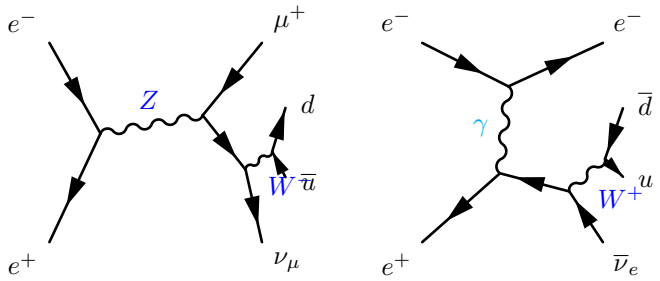

Figure 4: Non signal-like contributions to the WW cross-section, such that, a pair of final state particles are not constrained to the W mass distribution. The right-most diagram shows the electron channel dominant contribution to mirrored initial state helicites and gives a significant boost to the overall WW cross-section in the e channel.

unknown. These features create a significant challenge discovering new physics as well as producing precision physics measurements. The next frontier in high energy physics is through electron and positron collisions. These types of collisions are amenable to precision measurements because the process has a well defined initial state, less pile-up, and no excessive backgrounds from hadron collisions. The last major electron-positron collider was LEP, reaching center of mass energies of around 200 GeV which was replaced by the LHC in 2001. The ILC, featured in Figure 5, is the next proposed future linear collider which would harness center of mass energies from 200 GeV up to a possible 1 TeV upgrade. The proposed design was originally to start at 500 GeV center of mass energy along a 30 km linear accelerator(linac). Cost awareness and the Higgs discovery have pushed the starting center of mass energy to 250 GeV with a 20 km linac with possible 500 GeV and 1 TeV upgrades as well as luminosity upgrades. The starting instantaneous luminosity planned to be achieved is 1.35×10^{34} cm^{-2}s^{-1}, leading to an integrated luminosity of 2 ab^{-1} after a decade. The accelerator will have tunable beams that can be polarized to predominatly LR,RL,RR,LL collisions. [4] A detailed description of the accelerator design can be found in the Technical Design Report [5].

3.2 Detector Description

There are two proposed detectors at the ILC which serve the same interaction point with a push-pull mechanism. One detector will take data while the other is under maintenance. This allows for continuous collection of data, the opportunity for complementary detector designs, competition between detector experiments, and cross-checks between experimental results. All with the benefit of lower overall cost since there is only a single interaction point(IP). The two proposed detectors are the International Large Detector(ILD) and the Silicon Detector(SiD). The ILD concept is feautured in Figure 6. The accelerator's two opposing beams meet in the center of

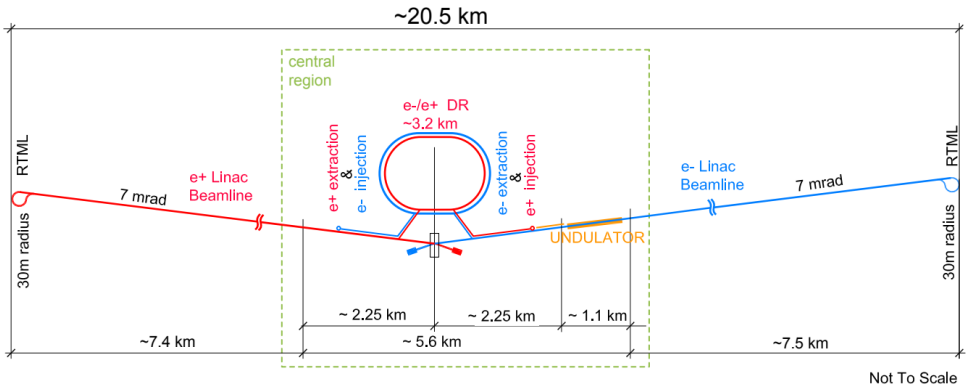

Figure 5: Schematic layout of the ILC in the 250 GeV staged configuration [4]

a detector and collide. The collision products then travel outward through the detector. The detector components form a shell around the beam line and each layer has a specific role in detecting types of particles. The detector layers from the innermost to outermost are a vertex detector used to identify the origin of an event, the tracker which measures the momentum of charged particles, an electromagnetic calorimeter(ECAL) which measures the energy deposited by less massive particles and photons, a dense hadronic calorimeter(HCAL) which stops and contains the showers from more massive particles, a solenoid which produces a magnetic field bending the trajectory of charged particles in order to distinguish charge, and an external muon layer which detects muons. The forward regions also have a collection of calorimeters designed to capture beam particles scattered at small angles. Both detectors optimize reconstruction of particles by the use of the Particle Flow Algorithm(PFA). The PFA is a method that combines algorithms and a highly granular calorimeter to fully resolve individual particles and their energy deposits [6]. The ILD approach to PFA optimization is by making the detector large, thus creating more physical separation between particles making reconstruction easier. The SiD approach is towards cost efficiency with a smaller detector and stronger magnetic field to try and achieve a similar performance. The major difference between the two detectors are the tracking mechanisms. ILD plans to use a gaseous central tracker with Time Projection Chamber(TPC). This tracking approach provides nearly continuous path information for tracks by providing up to 224 hits per track. SiD plans to use a silicon tracking system similar to the LHC. The design demands for both detectors are as follows: at least 4 μm spatial resolution in the vertex detector , a momentum resolution $\Delta(1/p) = 2 \times 10^{-5}$ GeV^{-1}, a jet energy resolution of at least 3%, and hermeticity specifically to capture and detect the momentum from particles in the forward region benefitting analyses driven by missing energy [4].

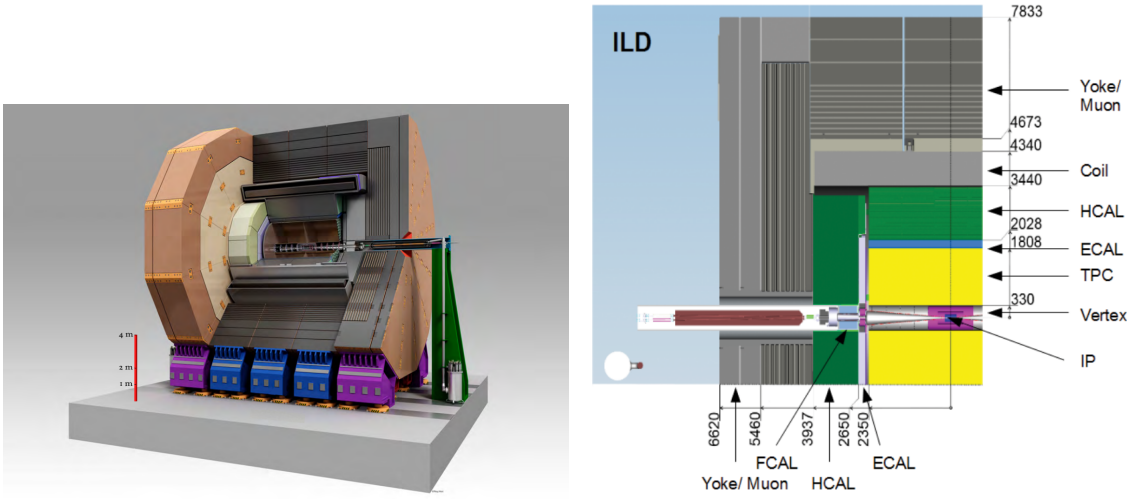

Figure 6: The ILD concept(Left). Quadrant slice of ILD and components, dimensions in mm (Right) [7].

3.3 Software Packages

The software ecosystem for the ILC is contained under iLCSoft [8] which is comprised of reconstruction tools that rely on the event data model LCIO [9]. Full simulation samples that are generated are based on detector descriptions in DD4HEP [10]. The physics samples are centrally produced with the Whizard event generator [11] and simulated in the detector with Geant4 [12].

4 Measurement of the W mass and Cross-section

4.1 Analysis Overview

The analysis relies on Monte Carlo events that are fully simulated using the ILD detector model `ILD_l5_o1_v02` with iLCSoft version v02-00-02 and includes a complete standard model background for final states with 2, 4, and 6 fermions as well standard model Higgs production. A center of mass energy of 500 GeV and longitudinally-polarized beams in various operating scenarios are considered. The Monte Carlo events are generated for 100% polarized beams, that is, either all left or right handed. Events are weighted in order to obtain realistic cases of partial polarizations for the possible running scenarios which are shown in Table 2.

The fraction of the beam, which is either left or right handed, is related to the

Table 2: Possible running configurations with partial longitudinal beam polarizations (P_{e^-}, P_{e^+}) and integrated luminiosity [13]

Pol.	(-0.8,+0.3)	(+0.8,-0.3)	(-0.8,-0.3)	(+0.8,+0.3)
$\int$ Lum. [fb^{-1}]	1600	1600	400	400

the partial polarizations P_{e^-} P_{e^+}

$$\begin{aligned} f_R^{e^-} + f_L^{e^-} = 1, \quad f_R^{e^-} = \frac{1}{2}(1 + P_{e^-}), \quad f_L^{e^-} = \frac{1}{2}(1 - P_{e^-}) \\ f_R^{e^+} + f_L^{e^+} = 1, \quad f_R^{e^+} = \frac{1}{2}(1 + P_{e^+}), \quad f_L^{e^-} = \frac{1}{2}(1 - P_{e^-}) \end{aligned} \tag{3}$$

where the beam fraction f is denoted with the polarization subscript and respective beam superscript. For a particular scenario like $(P_{e^-}, P_{e^+}) = (-0.8, +0.3)$ the -0.8 represents an electron beam with 90% left handed electrons mixed with 10% right handed electrons and a positron beam with 65% right handed positrons mixed with 35% left handed positrons. The weight ω for a specific event with particular initial state helicities is given by (with example partial polarizations (-0.8,+0.3)):

$$\begin{aligned} \omega_{LR} &= f_L^{e^-} f_R^{e^+} = 0.9 \times 0.65 = 0.585 \\ \omega_{RL} &= f_R^{e^-} f_L^{e^+} = 0.1 \times 0.35 = 0.035 \\ \omega_{LL} &= f_L^{e^-} f_L^{e^+} = 0.9 \times 0.35 = 0.315 \\ \omega_{LR} &= f_R^{e^-} f_R^{e^+} = 0.1 \times 0.65 = 0.065 \end{aligned} \tag{4}$$

The analysis workflow for semileptonic WW has three distinct stages, the lepton identification and selection, pile-up rejection in the hadronic system, and event selection against full standard model backgrounds. The analysis is performed with the running scenario that creates the most dominant WW production mode (-0.8,+0.3).

4.2 Lepton Identification

The approach towards the identification of leptons relies on treating leptons universally. The easiest lepton to identify is the muon, which produces a single track along with hits in the muon detector. The electron also produces a track in the TPC but is often accompanied by photons via bremsstrahlung radiation. The tau is the most difficult lepton to identify due to its frequent decay into multiple charged and neutral particles. To accommodate all types of lepton signature, a cone based approach is used to either capture single tracks or collimated jets with low track multiplicity. The lepton finding cone is based on the TauFinder package [14] designed for the Compact

Linear Collider(CLIC). TauFinder consists of two major structures, a search cone containing the particles that belong to the lepton candidate and an isolation cone whose purpose is to reject a lepton candidate if the search cone is not well-isolated from other particles. The acceptance criteria for a search cone consists of these parameters:

- Search cone angle α - The opening (half) angle of the search cone for the lepton jet [rad]
- Isolation cone angle β - The outer isolation cone angle w.r.t to the search cone [rad]
- Isolation energy - The total energy allowed within the isolation cone region [GeV]
- Invariant Mass - The upper limit on the lepton candidate mass [GeV]
- Track multiplicity - The allowed number of tracks in a lepton candidate
- Minimum P_t seed - the minimum transverse momentum of a track that seeds a lepton candidate [GeV]

An example of the cone and parameters are shown in Figure 4.2. Additional requirements are imposed on all of the reconstructed Particle Flow Objects(PFOs) in the event in order to suppress pile-up particles being included in the lepton jet.

- $P_t > 0.2$ GeV
- $|cos\theta| < 0.99$

The formation of a lepton candidate follows three steps (1) candidate construction, (2) candidate merging, and (3) isolation testing. The first step starts with seed tracks that are sorted by energy in descending order. Any track or neutral particle that falls within the search cone of the lepton candidate is added to the lepton candidate. For each newly added particle, the energy and momentum of the lepton candidate is updated. Each candidate has a unique set of particles. Lepton candidates are continually formed until the seed tracks are exhausted. When there are no more candidates to be created, the candidates are subjected to part of the acceptance criteria: the lepton jet mass is required to be below the upper mass limit (2 GeV) and the number of charged tracks within the lepton candidate is non-zero and less than or equal to 4. If a lepton jet violates any acceptance conditions it is deleted. The next step in the process is merging. If two lepton candidates form an opening angle of less than 2α, the candidates are merged. If the mass or track multiplicity conditions are violated, both lepton candidates are deleted. All candidates that survive merging are subjected to the isolation testing. For each candidate, the sum of energy of all the particles

that fall inside the isolation cone is computed. If the total energy inside the isolation cone is greater than the maximum allowed energy inside the isolation cone the lepton candidate is deleted.

The universal lepton treatment is not conducive to a one size fits all approach to lepton ID due to the abundance of different lepton signatures. To accommodate variations between lepton signatures, the acceptance criteria for leptons is optimized according to lepton flavor and τ decay mode. The categories created are:

- Prompt μ
- Prompt e
- $\tau \rightarrow \mu\overline{\nu_\mu}\nu_\tau$
- $\tau \rightarrow e\overline{\nu_e}\nu_\tau$
- $\tau \rightarrow$ hadrons (1-prong)
- $\tau \rightarrow$ hadrons (3-prong)

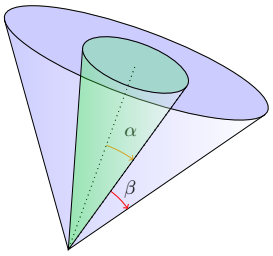

Figure 7: Illustration of possible lepton candidate cone with search cone angle α and isolation cone angle β. The search cone is shown in green and the isolation cone is the surrounding blue cone.

The Prompt categories refer to events in which the leptonic W decays directly to either a muon or electron and associated neutrino. The tau categories address the various dominant decay modes of the tau lepton. The optimal lepton acceptance criteria are calculated for each category. The optimal acceptance criteria is the set of parameters that maximally identify lepton candidates that originate from true leptons and minimize the fake lepton candidates that originate from hadronic jets. To find this set of parameters, a scan over a 3D space is performed using the search cone-α, isolation cone-β, and isolation energy-E_{iso}. The invariant mass is held at a fixed 2 GeV for simplicity. Two parameters are defined to find the optimal working point in the lepton finding space. The first is related to correctly identifying jets originating from true leptons. This is denoted as the efficiency of reconstructing a true lepton ϵ_T. The second optimization parameter is denoted as P_F, the probability of a fake lepton jet arising from a single hadronic jet, which is related to the efficiency of of reconstructing a fake lepton ϵ_F.

$$\epsilon_T = N_{match}/N_{Stotal} \tag{5}$$

$$P_F = 1 - (1 - \epsilon_F)^{\frac{1}{4}}$$
$$\epsilon_F = N_{fake}/N_{Btotal} \quad (6)$$

The true lepton reconstruction efficiency is maximized with the signal sample $WW \to q\bar{q}\ell\nu$. The denominator represents the total, category specific, number of events which contain three generator visible fermions. The true $q\bar{q}\ell$ fermions are required to fall within the acceptance range $|cos\theta| < 0.99$. N_{match} is the number of signal sample events in which a lepton candidate is reconstructed and can be matched to the true lepton, such that the opening angle between the reconstructed lepton and the true lepton is less than 0.1 radians. The distribution of opening angles is show in Figure 8. In the case that a reconstructed lepton is being matched to a true tau, the matching angle is formed between the reconstructed lepton and the vector sum of the visible generator components of the tau decay. The visible components of the tau decay consist of the direct decay products whereas photons from final state radiation of the tau prior to decay are excluded. The fake lepton probability P_f is minimized using the background sample $WW \to q\bar{q}q\bar{q}$ and is a function of the fake lepton reconstruction efficiency ϵ_F. The denominator for fakes is also subjected to the same acceptance range $|cos\theta| < 0.99$ for all four fermions. The numerator is the total number of events that contain at least one reconstructed fake lepton. The fake efficiency can be interpreted as the binomial probability of r-successes(lepton reconstructions) in 4 trials(hadronic jets). The probability of a single success in a single trial, P_F, can be directly derived from the binomial p.d.f using the fake efficiency ϵ_F per hadronic jet. The optimal parameters α, β, E_{iso} for each lepton category are extracted from $\max[(1 - P_F)\epsilon_T]$. The results for each category are shown in Table 3.

Since only one lepton is expected from signal, a single lepton candidate is selected as the candidate for the event. If multiple lepton jets are reconstructed then the lepton candidate with the highest energy is selected as the single candidate for the event. Any additional lepton candidates are treated as part of the hadronic system. The energy distribution of true and fake leptons is shown if Figure 9.

4.3 Pileup mitigation

After a lepton candidate has been selected, the remaining particles in the system are expected to form the hadronically decaying W boson. However, the vector sum of the particles produces a distribution that is often in excess of the true hadonic mass. Variation between the true and measured mass naturally arises due to the mismeasurment of particles – especially neutral hadrons, as well as particles lost beyond the acceptance of the detector. Neither of these effects should create a systematic excess in the hadronic mass. The nature of the excess can be understood through the kinematics of the WW in the LR and RL configurations shown in Figure 10 and 11.

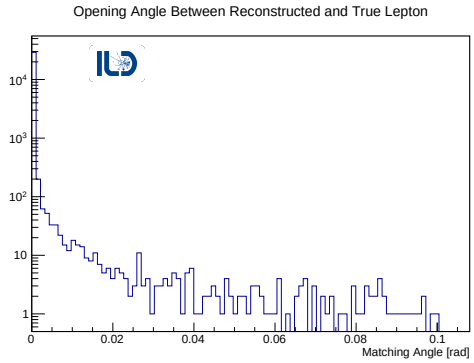

Figure 8: Distribution of opening angles between the closest reconstructed lepton candidate and the true muon from $WW \to q\bar{q}\mu\nu_\mu$. 99.4% of events with a muon candidate are matched to truth.

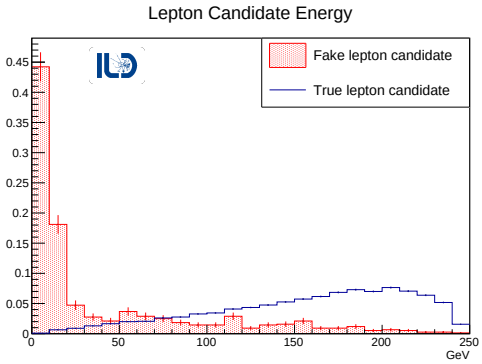

Figure 9: Energy distribution of lepton candidates matched to truth from $WW \to q\bar{q}\mu\nu_\mu$ and fake candidates from $WW \to q\bar{q}q\bar{q}$ both normalized to unity.

Channel	n Lep ≥ 1 (%)	$1 - P_F$ (%)	ϵ_T (%)	Search-Cone [rad]	Iso.Cone [rad]	Iso.E [GeV]
Prompt μ	95.5 ± 0.3	97.4 ± 0.1	94.9 ± 0.3	0.03	0.15	3.0
Prompt e	92.0 ± 0.3	96.1 ± 0.1	90.4 ± 0.3	0.04	0.15	4.0
Inclusive τ	80.0 ± 0.5	94.3 ± 0.1	77.0 ± 0.6	0.07	0.15	4.5
$\tau \to \nu\nu\mu$	81.5 ± 1.2	97.4 ± 0.1	80.1 ± 1.3	0.03	0.15	3.0
$\tau \to \nu\nu e$	80.0 ± 1.2	96.3 ± 0.1	78.1 ± 1.3	0.05	0.15	3.5
τ Had-1p	74.4 ± 0.9	93.0 ± 0.2	70.7 ± 0.9	0.07	0.15	4.5
τ Had-3p	75.6 ± 1.5	93.0 ± 0.2	71.0 ± 1.6	0.07	0.15	5.5

Table 3: Optimization results using 100% LR $q\bar{q}\ell\nu$ and $q\bar{q}q\bar{q}$ samples. The n Lep ≥ 1 column pertains to signal samples where at least one lepton candidate was found and is not subjected to the truth matching criterion of 0.1 radians. Results shown are the configurations that maximize $(1 - P_F)\epsilon_T$.

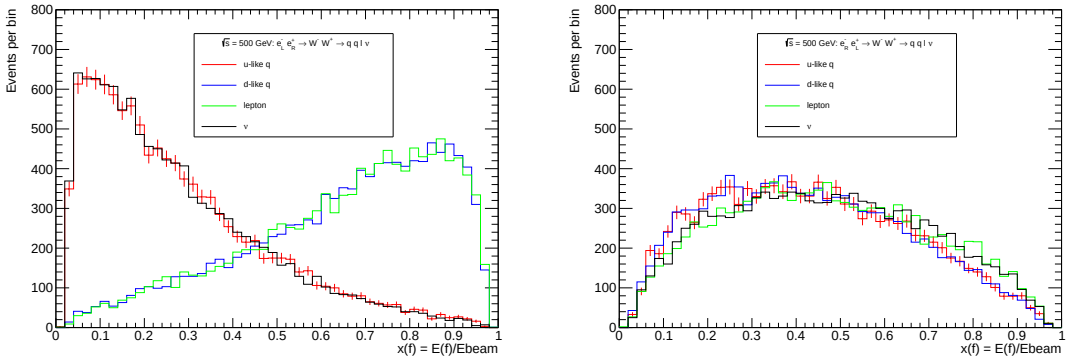

Figure 10: The fractional energy partitioning of the true fermions with $\ell = \mu, \tau$, 100% polarization for the initial state helicities LR(Left) and RL(Right) at center of mass energy 500 GeV. In the LR configuration the charged lepton and down-like quark take the majority of the beam energy. In RL the energy partitioning is even between the four fermions.

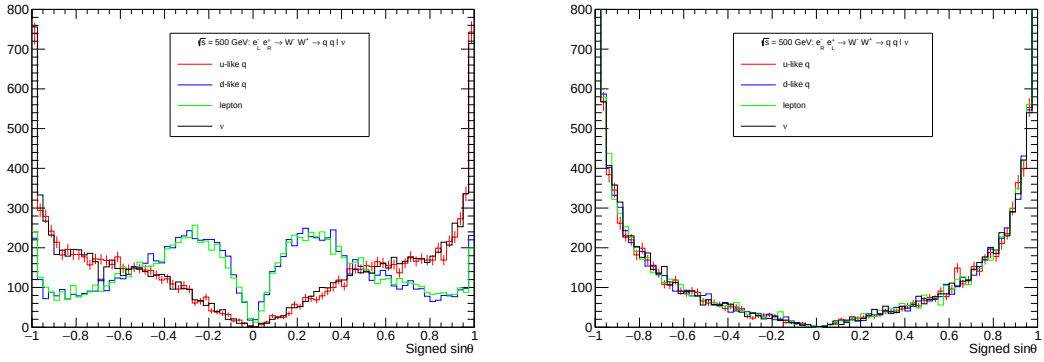

Figure 11: The Signed sine of the polar angle of the true fermions with $\ell = \mu, \tau$. 100% polarization for the initial state helicites. The sign of $sin\theta$ corresponds to the sign of $cos\theta$. As $sin\theta \to 0$ the fermion is forward in the detector but for $|sin\theta| \to 1$ the fermions become maximally transverse to the beam. In the LR configuration(Left) the charged lepton and down-like quark are scattered forward while the up-like quark and neutrino are ejected centrally into the detector. In the RL configuration(Right) all of the fermions are more centrally produced.

The highest yielding configuration, LR, typically has two fermions that are forward in the detector which both typically have a large fraction of the beam energy. These fermions are susceptible to pile-up scattering into the detector and mixing directly into the reconstructed jets. To combat effects of pile-up, jet clustering algorithms via FastJet [15] are used. The standard approach for pileup mitigation is to use the k_T algorithm [16] and tune the R parameter such that the pile-up particles are associated with beam jets while the desired particles are not. With successful k_T clustering the beam jets can be thrown away without damaging the reconstruction of the desired event. However, this approach only works well in events that are centrally produced. The pile-up overlap in the forward topology with the k_T algorithm based clustering leads to rejecting desired particles and severe undermeasuremnt of the W mass. The solution to proper pileup mitigation is through the precise removal of foreign particles inside the reconstructed jets. This can be achieved by using the standard JADE algorithm and mass based cut-off parameter $y_{cut} > y_{ij}$ where $y_{ij} = M_{ij}^2/Q^2$ with M_{ij} being the invariant mass of the pair of objects being combined and Q^2 being the visible energy in the e^+e^- annihilation [17]. The mass of individually reconstructed jets can be controlled by tuning the y_{cut} parameter. For large values, $y_{cut} = 1 \times 10^{-3}$, a single massive jet is reconstructed. In the limit that y_{cut} becomes infinitely small the number of jets reconstructed converges to the number of reconstructed particles. The best y_{cut} value is the value that forms mini-jets that safely couple together hard and soft emissions from the original quark jet while segregating pile-up into its own mini-jets. The mini-jets are then subjected to kinematic cuts that maximize the pileup rejection and minimize the difference between the true and measured hadronic W mass. The best combination of y_{cut} and mini-jet kinematic cuts are found by examining the 100% polarized LR signal dataset for $qq\mu\nu$. Two statisical estimators are used to maximize the pile-up rejection, both of which come from the distribution of $M_{qq}^{meas} - M_{qq}^{true}$. This binned mass difference distribution is created from the subset of mini-jets that arise from clustering with a given y_{cut} and also pass some jet veto cuts $p_{Tjet} > x$ and $|cos\theta_{jet}| < y$. The estimators, from the distribution, are the Full Width Half Maximum(FWHM) and the number of entries in the Mode. Using estimators calculated from a binned histogram creates unwanted sensitivity to bin size. To reduce sensitivity to binning, the mode is defined as the bin with the most entries. The "mode entries" is the number of entries in the mode bin plus the number of entries in the mode bins nearest neighbors. For the FWHM, the mass distribution is assumed to be monotonically decreasing around the half maxmimum. To create a more sensitive continuous distribution of the FWHM, the FWHM is weighted towards the bin center of the two bins around (above/below) the half maximum. The results of the optimization are shown in Figure 13 and various y_{cut}'s are shown in comparison to the optimal configuration in Figure 12. The optimal result uses $y_{cut} = 5 \times 10^{-5}$, mini jet $P_T > 2$ GeV, and has no $|\cos\theta|$ requirement.

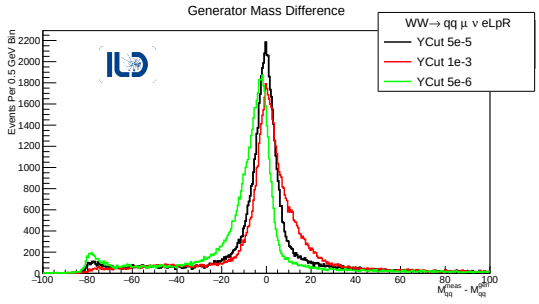

Figure 12: Comparison of mass difference distributions with different y_{cut} values and the same mini-jet cut $P_T > 2$. $y_{cut} = 1 \times 10^{-3}$ results in massive jets that are not separated from pile-up and insensitive to small kinematic cuts. $y_{cut} = 5 \times 10^{-5}$ has the best balance between jet clustering and mini-jet cuts. $y_{cut} = 5 \times 10^{-6}$ yields a highly fragmented version of the jets where the mini-jets are not distinguishable from pile-up and are thrown out, resulting in the small peak around -80 GeV where the hadronic W is completely thrown out.

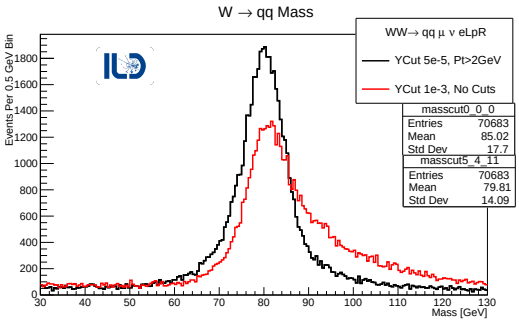

Figure 13: The increase of quality of the hadronic mass is shown between the red curve which is the raw hadronic system after lepton identification versus the black curve which is subjected to the pile-up mitigation with $y_{cut} = 5 \times 10^{-5}$ and mini jet $P_T > 2$ GeV. On average the excess in mass is reduced by ≈ 5 GeV.

4.4 EventSelection

The W-pair selection has been optimized for a Monte Carlo sample of 1600 fb^{-1} with the $(-0.8, +0.3)$ beam scenario and is based on the selection in [18]. The selection includes the full 2,4,6 fermion and Higgs SM background, and is performed with two mutually exclusive subsets, a tight and loose selection. The tight selection uses the prompt muon cone to identify signal events that contain both prompt and non-prompt muons and electrons. The tight selection is inefficient in collecting hadronic taus, so, the loose selection, using the inclusive tau cone, is designed to recover the efficiency of hadronic taus and other problematic events. The selection criteria is applied after the pileup mitigation and is as follows:

- N Leptons ≥ 1
- Track Multiplicity > 10
- Visible Pt > 5 GeV
- $E_{vis} < 500$ GeV
- $E_{com} > 100$ GeV
- $40 < M_{qq} < 120$ GeV
- $-qcos\theta_W > -0.95$
- $m^{vis2}_{recoil} < 135,000$ GeV^2

The track multiplicity and E_{com} target 2 fermion backgrounds. E_{com} is the rest-frame energy that consists of the visible and inferred missing energy. The missing energy is treated as a single neutrino with zero mass such that $E_{com} = E_{vis} + |P_{miss}|$ and $P^{\mu}_{miss} = (|P_{miss}|, -\sum \vec{p}_{vis})$. The visible P_T is the magnitude of the vector of all measured transverse momenta and E_{vis} is the sum of all reconstructed visible energy in an event. The P_T and E_{vis} cuts target processes that do not have a genuine missing energy from a neutrino. The hadronic W-mass M_{qq} requirement forces the hadronic system to be "W-like" and the recoil mass, $m_{\nu recoil}$, uniquely requires the visible system to be recoiling against an invisible system with little to no mass. The recoil mass is defined as $m^2_{\nu recoil} = s + M^2_{vis} - 2\sqrt{s}E_{vis}$ and $M^2_{vis} = (P^{\mu}_{qq} + P^{\mu}_{\ell})^2$. The W-scattering angle $-q\cos\theta_W$ is the angle of deflection of the system identified as W^- with respect to the e^- beam axis and is implemented to limit backward scattering. The charge of the lepton is extracted from the leading momentum track from candidates with 1, 2, or 4 tracks, or in the case of 3 tracks, the charge is the sum of the three track charges. The hadronic system is then tagged with the opposite charge. This procedure results in the correct charge assignment of the lepton before selection

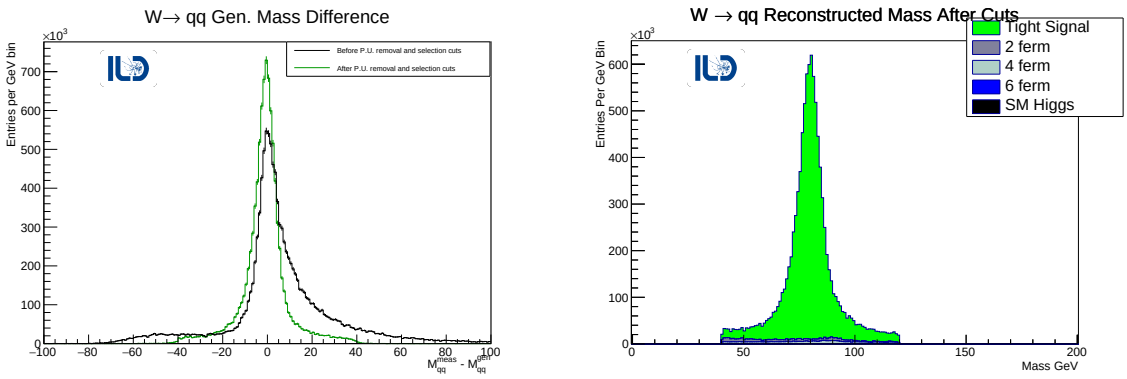

Figure 14: The right distribution is the mass of the hadronic W-boson after pile up removal and selection cuts against the remaining background events . The left distribution shows the resolution of the hadronic W mass with respect to the true mass in Monte Carlo before pile up removal and selection cuts and after pile up removal and selection cuts. The resolution shows a significant improvement in symmetry and events with excess mass are shifted centrally. Uses 1600 fb^{-1} in (-0.8,+0.3).

cuts for about 98.9% of prompt muons, 94.8% of prompt electrons, and 95.9% of taus. Following the event selection the correct charge assignment increases to 99.9% for prompt muons, 98.3% for prompt electrons, and 98.8% for taus. The details of the tight and loose selection for (-0.8,+0.3) at 1600fb^{-1} are summarized in Table 4. The selections in Table 4 differ by the veto of the tight lepton in the loose selection, where the preference for any event is to always choose a tight lepton over loose. The primary selection also includes only "WW-like" signal, this type of signal is such that both of the true fermion pairs invariant masses are each within ±10 GeV of the nominal W mass. If an event contains a fermion pair that is outside the WW-like range, it is designated as an off-shell(O.S) event and is placed in a different category. The selection cuts are optimized to maximize the efficiency and purity of the total signal for the tight selection. The results are summarized with the two selection cones with and without O.S. events in Table 5. The final results for the mass inclusive selection yields a signal efficiency of 58% with only a 9% of background contaminating selected events. The W-boson invariant mass after selection is shown with mass resolution in Figure 14

4.5 Results

A fit with the convolution of a Breit-Wigner with a Gaussian (Voigtian) of the hadronic W mass is performed on the tight signal sample with the combined lepton categories shown in Figure 15. The resulting fit models the shape and the mean of the distribution well but deviates around 90 GeV the and edges of the fit win-

Table 4: The tight and loose selection for 1600 fb^{-1} (-0.8,+0.3). The tight selection is most efficient with prompt leptons with 69% and 65% for muons and electrons respectively, but struggles to efficiently reconstruct taus. The loose selection recovers 10% of the tau efficiency and is inefficient for prompt leptons because of the tight lepton veto. The tight lepton veto enforces the orthogonality of the selections and gives preference toward better lepton candidates. The signal categories Base Evts. only include events in which the true W mass of both fermion pairs are within 10 GeV of the nominal W mass.

Tight selection with muon cone

($\times 10^5$)	$qq\mu\nu$	$qqe\nu$	$qq\tau\nu$	Tot. Sig.	2f	4f	6f	Higgs
Base Evts	38.7	38.9	39.0	117	422	322	2.14	4.12
Lepton	33.1	32.0	22.8	87.8	115	118	1.63	1.15
E_{vis}	32.8	31.1	22.7	86.7	106	115	1.62	1.11
N Tracks	31.9	30.3	22.1	84.3	25.4	25.9	1.49	0.889
$-qcos\theta$	31.8	30.1	21.8	83.7	21.9	22.6	1.44	0.852
M_{qq} >40	29.4	28.0	20.3	77.7	11.3	13.3	1.42	0.756
M_{qq} <120	27.2	25.7	18.3	71.3	5.68	2.68	0.202	0.297
E_{com}	27.2	25.7	18.3	71.3	5.58	2.65	0.202	0.296
Pt vis.	26.9	25.5	18.1	70.5	3.21	2.37	0.201	0.294
$m^2_{\nu recoil}$	26.9	25.4	18.0	70.3	2.93	2.02	0.194	0.223
ϵ (%)	69.4	65.4	46.2	60.3	0.69	0.626	9.05	5.41
	±0.2	±0.2	±0.3	±0.2	± 0.01	± 0.008	± 0.02	±0.05

Loose selection with tau cone

($\times 10^5$)	$qq\mu\nu$	$qqe\nu$	$qq\tau\nu$	Tot. Sig.	2f	4f	6f	Higgs
Base Evts	38.7	38.9	39.0	117	422	322	2.14	4.12
Lepton	33.6	33.0	28.2	94.8	130	136	1.77	1.38
Tight Veto	0.772	1.28	5.70	7.76	19.3	21.5	0.161	0.312
E_{vis}	0.764	1.26	5.70	7.72	18.2	19.4	0.154	0.302
N Tracks	0.737	1.21	5.54	7.49	15.0	16.4	0.151	0.271
$-qcos\theta$	0.630	1.12	5.32	7.07	11.1	14.1	0.145	0.256
$M_{qq} > 40$	0.492	0.972	4.86	6.33	5.98	13.0	0.144	0.233
$M_{qq} < 120$	0.404	0.781	4.16	5.35	2.58	1.11	0.0111	0.124
E_{com}	0.404	0.781	4.16	5.34	2.50	1.10	0.0111	0.124
Pt vis.	0.400	0.774	4.12	5.29	1.17	1.01	0.0111	0.123
$m^2_{\nu recoil}$	0.394	0.770	4.07	5.24	1.02	0.759	0.0102	0.0973
ϵ (%)	1.02	1.98	10.5	4.49	0.241	0.236	0.474	2.36
	±0.5	±0.07	±0.2	±0.07	±0.003	±0.004	±0.007	±0.02

Table 5: Selection summary showing the number of background events that pass the event selection, efficiency, and purity for the tight selection or combined selections and with or without the off-shell contributions. The O.S. contributions are less efficiently reconstructed so their inclusion reduces the overall signal efficiency but boosts the purity by increasing the base number of signal events that can be selected. Selection is performed with 1600 fb^{-1} in (-0.8, +0.3).

	Tight Selection			Tight + Loose Sel.		
	Sel. Total ($\times 10^5$)	Efficiency (%)	Purity (%)	Sel. Total ($\times 10^5$)	Efficiency (%)	Purity (%)
Bkg.	5.36			7.25		
Signal	70.3	60.3 ± 0.2	92.9	75.5	64.6 ± 0.2	91.2
Sig.+O.S.	93.6	56.0 ± 0.1	94.6	100.3	60.0 ± 0.1	93.3

dow. The width of the fit is also in excess of the true width, which is about 2 GeV. This means the Voitigian model is inadequate in describing the data, but, because the shape is similar to data, the fitted model is used to understand the achievable mass resolution given a perfect model. Statistics consistent with 1600 fb^{-1} (9.36M Events) are produced according to the previously fitted model with a mean $M_W = 79.7074$ GeV, width $\Gamma_W = 10.6972$ GeV and $\sigma_W = 4.847 \times 10^{-7}$ GeV and refitted to achieve the statistical error on the mean $\Delta M_W(\text{stat.}) = 2.4$ MeV with goodness-of-fit $\chi^2/ndof = 67.8/77$. The toy model refit is also included in Figure 15. The cross-section and errors are extracted from Table 4 according to the formula:

$$\sigma = \frac{N_T - N_B}{L\epsilon} \tag{7}$$

where N_T is the observed number of events that passes selection and N_B is expected number of background events that contaminate the signal selection. The resulting statistical error on the cross-section with ϵ, L, and N_B known perfectly is $\frac{\Delta\sigma}{\sigma} = 0.04\%$. Combining the errors for efficiency, Poisson errors for N_T, and having no background contribution, the resulting cross-section obtained in the combined selection is 7994 ± 14 fb

5 Discussion and Conclusions

The results show a promising start to potential electroweak precision measurements for the ILC with the statistical error on the mass of $\Delta M_W(\text{stat.}) = 2.4$ MeV from a full detector simulation study. Such a measurement is very competitive with the current PDG measurement of $\Delta M_W = 12$ MeV, ass uming that systematic uncertainties can be sufficiently controlled. Another ILC study of the W mass showed

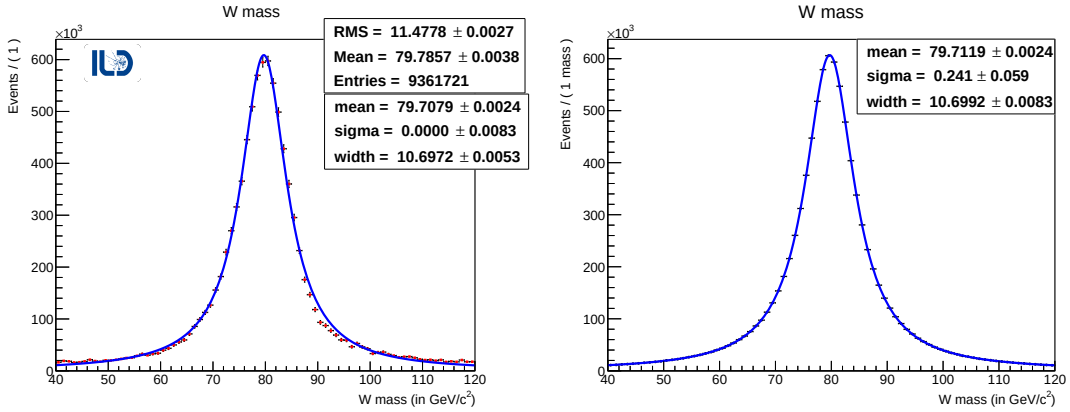

Figure 15: The left distribution shows the (-0.8,+0.3) W mass distribution for all signal after selection cuts. The fit results in the Voigtian parameters $M_W = 79.7074$ GeV, width $\Gamma_W = 10.6972$ GeV and $\sigma_W = 4.847e-7$ GeV with Monte Carlo statistics scaled up to 1600 fb^{-1}. The right distribution shows the refit with 9.36M W's generated according to the fitted model.

that the achievable statistical error is $\Delta M_W(\text{stat.}) = 1.6$ MeV assuming an effective Gaussian mass resolution $\sigma_W = 4$ GeV per 10^7 hadronic W's [19]. The estimated uncertainties at ILC250 provide a limit on the resolution of the W-mass in ILC500 being $\Delta M_W = 3.7$ MeV. The mass measurement at ILC500 is more challenging because the W pair overlapping with pile-up is not a major issue at lower of center of mass energies. The equivalent precision may be unobtainable at higher $\sqrt{s}$, but propagating the same systematic error on the W mass for this study yields $\Delta M_W = 4.6$ MeV. Both measurements, however, are dominated by the systematic uncertainties from the effective jet energy scale which is a challenging demand. The statistical error on the cross-section also shows the utility of semileptonic WW as a method to precisely measure the beam polarization at the interaction point. This offers an important alternative for correctly measuring processes that are sensitive to beam polarization and assists in quantifying beam depolarization from collisions.

The lepton identification and charge assignment performance is exceptional with an overall correct charge assignment with 98.8% over all three channels. This has the biggest impact on the measurement of charged triple gauge couplings that rely on the identification of the W^-. The lepton identification itself, still has room for improvement in ways such as (1) a multivariate type approach with TauFinder and (2) re-optimization of the parameters over a mixed polarization beam-scenario which involves both LR and RL events. The optimization of the TauFinder parameters also led to every isolation cone for each category to choose 150 mrad, which is indicative of not achieving a global minimum. However, allowing the isolation to grow wider could mean overtuning the lepton identification to the topologies specific to LR.

The pileup mitigation is a mostly unexplored avenue of reconstruction in ILC500 as most processes are produced centrally or are not simulated with pile-up. The techniques developed to remove pile-up are optimized for W mass measurement, but, can be easily adapted to general usage in any type of process where the standard approaches for pileup removal are inadequate.

The event selection can also be improved. Additional cuts were explored such as the leptonic W mass, or maximum track multiplicity. The leptonic W mass cut best motivates the categorization approach of WW-like and not WW-like types of event, but, this cut, and others mentioned do not improve the overall efficiency times purity of the analysis. Specifically, the leptonic W mass can be improved and applied to event selection by using a more sophisticated calculation for the neutrino momentum. This can be done taking into account potential ISR in the z-direction, and applying a kinematic fit with constraints on the energy, momentum, and equal W masses. These adjustments would significantly improve the measured leptonic W mass and enhance the performance of the event selection, but requires well modeled uncertainities, and was beyond the scope of this work.

Some additional detector benchmarks can immediately follow the results of this analysis, one would be the quality of separation between prompt muons and tau muons to evaluate the performance of the vertex detector. Another study that should be done is examination of the analysis efficiency as a function of the polar angle, which tests the performance of the forward calorimeters. Overall, the semi leptonic analysis offers keen insights to analysis performed in an electron positron collider with $\sqrt{s} = 500$ GeV. The statistical errors on cross-section and mass are the first step but an important and tractable step in electroweak precision measurement at the ILC. The semileptonic channel still offers significantly more important physics in terms of TGC and polarization measurements in addition to expanding and improving the analysis presented here.

Acknowledgments

Thanks for comments and advice related to this project from Graham W. Wilson

References

[1] **Particle Data Group** Collaboration, "Review of particle physics," *Phys. Rev. D* **98** (Aug, 2018) 030001. https://link.aps.org/doi/10.1103/PhysRevD.98.030001.

[2] M. Thomson, *Modern particle physics*. Cambridge University Press, 2013.

[3] G. Moortgat-Pick, T. Abe, G. Alexander, B. Ananthanarayan, A. Babich, *et al.*, "The role of polarized positrons and electrons in revealing fundamental interactions at the linear collider, phys. rept. 460, 131–243 (2008)," *arXiv preprint hep-ph/0507011* .

[4] P. Bambade, T. Barklow, T. Behnke, M. Berggren, J. Brau, D. Denisov, A. Faus-Golfe, K. Fujii, J. Fuster, F. Gaede, *et al.*, "The international linear collider: A global project," 2019.

[5] C. Adolphsen, "The international linear collider technical design report-volume 3. ii: Accelerator baseline design," tech. rep., Argonne National Lab.(ANL), Argonne, IL (United States); Thomas Jefferson , 2013.

[6] J. Marshall and M. Thomson, "The pandora particle flow algorithm," *arXiv preprint arXiv:1308.4537* (2013) .

[7] T. Behnke, "The international linear collider technical design report-volume 4: detectors," tech. rep., Argonne National Lab.(ANL), Argonne, IL (United States); Pacific Northwest , 2013.

[8] R. Poeschl, "Software Tools for ILC Detector Studies," *eConf* **C0705302** (2007) PLE104. [,61(2007)].

[9] S. Aplin, J. Engels, F. Gaede, N. A. Graf, T. Johnson, and J. McCormick, "LCIO: A Persistency Framework and Event Data Model for HEP," in *Proceedings, 2012 IEEE Nuclear Science Symposium and Medical Imaging Conference (NSS/MIC 2012): Anaheim, California, USA, October 29-November 3, 2012*, pp. 2075–2079. 2012. `http://www-public.slac.stanford.edu/sciDoc/docMeta.aspx?slacPubNumber=SLAC-PUB-15296`.

[10] **CLICdp, ILD** Collaboration, A. Sailer, M. Frank, F. Gaede, D. Hynds, S. Lu, N. Nikiforou, M. Petric, R. Simoniello, and G. Voutsinas, "DD4Hep based event reconstruction," *J. Phys. Conf. Ser.* **898** no. 4, (2017) 042017.

[11] W. Kilian, F. Bach, T. Ohl, and J. Reuter, "WHIZARD 2.2 for Linear Colliders," in *International Workshop on Future Linear Colliders (LCWS13) Tokyo, Japan, November 11-15, 2013*. 2014. `arXiv:1403.7433 [hep-ph]`.

[12] S. Agostinelli, J. Allison, K. a. Amako, J. Apostolakis, H. Araujo, P. Arce, M. Asai, D. Axen, S. Banerjee, G. . Barrand, *et al.*, "Geant4a simulation toolkit," *Nuclear instruments and methods in physics research section A: Accelerators, Spectrometers, Detectors and Associated Equipment* **506** no. 3, (2003) 250–303.

[13] T. Barklow, J. Brau, K. Fujii, J. Gao, J. List, N. Walker, and K. Yokoya, "Ilc operating scenarios," *arXiv preprint arXiv:1506.07830* (2015) .

[14] A. Münnich, "Taufinder: A reconstruction algorithm for τ leptons at linear colliders," tech. rep., 2010.

[15] M. Cacciari, G. P. Salam, and G. Soyez, "Fastjet user manual," 2012.

[16] S. Catani, Y. L. Dokshitzer, M. H. Seymour, and B. R. Webber, "Longitudinally-invariant k-clustering algorithms for hadron-hadron collisions," 1993.

[17] Y. L. Dokshitzer, G. Leder, S. Moretti, and B. Webber, "Better jet clustering algorithms," 1997.

[18] I. Marchesini, *Triple gauge couplings and polarization at the ILC and leakage in a highly granular calorimeter*. PhD thesis, Hamburg U., 2011.

[19] K. Fujii, C. Grojean, M. E. Peskin, T. Barklow, Y. Gao, S. Kanemura, H. Kim, J. List, M. Nojiri, M. Perelstein, *et al.*, "Tests of the standard model at the international linear collider," *arXiv preprint arXiv:1908.11299* (2019) .